ORGANIC PROCESS RESEARCH & DEVELOPMENT
OPR&D
Article
Cite This: Org. Process Res. Dev. 2019, 23, 1960−1969
pubs.acs.org/OPRD

Incorporating Solvent-Dependent Kinetics To Design a Multistage, Continuous, Combined Cooling/Antisolvent Crystallization Process

Jennifer M. Schall, Gerard Capellades, Jasdeep S. Mandur, Richard D. Braatz, and Allan S. Myerson*

Department of Chemical Engineering, Massachusetts Institute of Technology, E19-502D, 77 Massachusetts Avenue, Cambridge, Massachusetts 02139-4307, United States

Supporting Information

ABSTRACT: Combined cooling and antisolvent crystallization enables crystallization of many pharmaceutical products, but its process design typically neglects solvent composition influences on crystallization kinetics. This paper evaluates the influence of solvent-dependent nucleation and growth kinetics on the design of optimal, multistage mixed-suspension, mixed-product removal (MSMPR) crystallization cascades. The ability to independently select temperature and solvent compositions in each stage of the cascade serves to greatly expand the attainable region for a two-stage cascade, with diminishing returns for additional stages. Failure to include solvent-dependent kinetics can result in simulating incorrect attainable regions, active pharmaceutical ingredient (API) yields, and crystal size distributions. This work also demonstrates that commonly employed crystallization process design heuristics, such as equal antisolvent addition and decreasing temperature in successive stages, can result in suboptimal process design if kinetics are strongly solvent dependent.

KEYWORDS: *continuous crystallization, optimization, MSMPR, kinetics, antisolvent crystallization*

INTRODUCTION

Antisolvent crystallization is frequently used to produce active pharmaceutical ingredients (APIs) that exhibit high heat sensitivity, weak solubility−temperature dependence, or polymorphism.[1−4] Processes requiring antisolvent crystallization may be enhanced further by employing combined cooling and antisolvent crystallization (CCAC).[5] Traditionally, most antisolvent and CCAC pharmaceutical crystallizations are batch processes. However, batch crystallization processes have limitations. Batch processes are associated with longer processing times, are cost- and labor-intensive, and have a tendency to produce APIs with an inconsistent final product quality.[6,7] As a result, a shift is occurring toward using continuous antisolvent crystallizers to decrease costs and increase control.[8−12] Mixed-suspension, mixed-product removal (MSMPR) crystallizers represent one form of continuous crystallizer that shows promise for continuous CCAC of APIs. When designed well, MSMPRs are well-mixed vessels that enable enhanced control of final product attributes, polymorphism, yield, and purity.[13−15]

Unfortunately, engineers and researchers currently lack a systematic and generalized approach for the MSMPR cascade design using kinetic parameters for antisolvent crystallization. Although procedures exist for regressing solvent-dependent kinetic (SDK) parameters from batch crystallization experiments, these experiments have severe shortcomings. First, batch crystallizations tend to undergo separate nucleation and growth events; in an MSMPR crystallizer, growth and nucleation occur simultaneously, competing to reduce supersaturation.[16] Second, batch experiments have limited use for predicting secondary nucleation, which is the dominant nucleation mechanism in an MSMPR crystallizer.[17] Solvent-dependent kinetic parameters must be regressed from continuous crystallization experiments for a proper antisolvent MSMPR crystallizer design. This is especially important for multistage crystallization cascades, as having the ability to operate at different temperatures and solvent compositions in each stage expands the steady-state process design space. As nucleation and growth rates vary as a function of the solvent composition, tuning the solvent composition in each stage of an MSMPR cascade allows a variety of final product attributes to be achieved using a small number of MSMPR crystallizers.

Previous studies of continuous antisolvent crystallization with MSMPRs focus on process design and optimization but tend to neglect the solvent dependence of growth and nucleation kinetics. Yang and Nagy optimized start-up procedures for CCAC MSMPR cascades, demonstrating that applying dynamic antisolvent and temperature profiles can reduce start-up time and waste by almost 50%.[18] Vetter et al. introduced the concept of the attainable region for MSMPR operation, which encompasses the set of operating conditions where mean product particle size can be obtained, subject to constraints on operating conditions.[19] When applied to a combined cooling and antisolvent crystallization (CCAC), bounds on the solvent fraction and temperature in each crystallizer restrict the size of the attainable region.[19] Wong et al. showed that incorporating recycle with the MSMPR crystallizer can reduce the need for multiple MSMPR crystallizers in a CCAC cascade.[20] Most recently, Da Rosa and Braatz presented openCrys, an open-source software for CCAC modeling of crystallizers with turbulent flow, emphasizing that the optimal crystallizer design is nonobvious because of the complex interplay between kinetics and transport phenomena.[21] The same complexity arises in the case of CCAC in MSMPR crystallization, as well. However, the

Received: May 24, 2019
Published: August 14, 2019

DOI: 10.1021/acs.oprd.9b00244
Org. Process Res. Dev. 2019, 23, 1960−1969

systems studied in each of these papers assumed that crystal nucleation and growth kinetics were invariant with respect to the solvent composition.

Studies of antisolvent crystallization indicate that beyond its impact on thermodynamics, solvent composition can have a substantial effect on crystallization kinetics. Regarding nucleation, Zhang et al. demonstrated that solution composition strongly influenced nucleation kinetics in the continuous antisolvent crystallization of a proprietary compound, affecting the optimal location of the antisolvent addition in the crystallization cascade.[22] Regarding growth, Garg et al. proposed a mechanistic modeling that incorporates both size-dependent and solvent-dependent growth kinetics to predict the mean particle size in a batch antisolvent crystallizer.[23] Recently, we demonstrated that growth and nucleation kinetics parameters can be profoundly influenced by solvent composition, as even small changes in solvent composition can drastically increase crystal growth and nucleation rates in a continuous MSMPR crystallizer.[24] To accurately predict performance in a single MSMPR crystallizer, the temperature and solvent dependence of the kinetics should be studied and incorporated in crystallization process design models.

To speed the CCAC MSMPR cascade design, it may seem intuitive to place additional constraints on the process optimization. This could include requiring equal mass deposition or production rates in each stage or requiring equal antisolvent addition (EAS) in each stage. Most commonly, a constraint is imposed to require the temperature to remain the same or decrease in each successive stage when designing continuous cooling or CCAC crystallization processes.[18,19,25,26]

In this work, the solvent-dependent and temperature-dependent kinetics for a proprietary API have been used to optimize a steady-state, *N*-stage MSMPR cascade. For this study, maximizing yield is the primary process objective for the model. The simulated crystallization process uses combined cooling and antisolvent crystallization and is subject to manufacturer-imposed process constraints. After determining the best set of operating conditions for each MSMPR crystallizer cascade, the attainable region for each cascade is simulated. These results are then compared to optimization results when solvent-dependent kinetics are neglected. Finally, for the case of the two-stage MSMPR cascade, the optimization results are compared to optimization results obtained if common MSMPR design heuristics are used. Two heuristics are evaluated: (1) where equal antisolvent addition volumes are added to each crystallizer and (2) where the temperature is required to remain the same or decrease in each stage. Ultimately, it is shown that the design of a CCAC MSMPR cascade process is nonobvious when solvent-dependent nucleation and growth kinetics are considered.

MATHEMATICAL MODELING

System Description. The API of interest for this study is a proprietary compound that was supplied by Novartis International AG. Throughout this work, this compound will be referred to as API. API is crystallized using a three-solvent system, where water is the antisolvent and a 92 vol % ethanol (EtOH)/ 8 vol % tetrahydrofuran (THF) solution is used as the solvent. Currently, API is manufactured using a batch crystallization process where the antisolvent is added to induce crystallization, then cooling occurs to increase the extent of crystallization. This batch process takes more than 12 h, so there is a great opportunity to reduce the processing time by developing a continuous process for this compound.

API exhibits solvent-dependent thermodynamics and kinetics, which were studied previously.[24] The solubility of API is a strong function of both temperature and solvent composition, as shown in Figure 1. Based on the previous

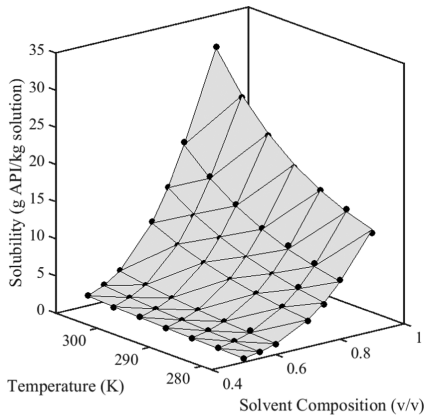

Figure 1. Solubility of API as a function of the solvent fraction and temperature.

findings, API solubility in stage i, c_i^*, is estimated using a modified Apelblat equation, as follows

$$\ln(c_i^*) = \left(\zeta_{11} + \zeta_{12}\nu_{s,i} + \frac{\zeta_{13}}{\nu_{s,i}} + \zeta_{14}\ln(\nu_{s,i})\right) + \frac{\zeta_{21} + \zeta_{22}\nu_{s,i} + \frac{\zeta_{23}}{\nu_{s,i}} + \zeta_{24}\ln(\nu_{s,i})}{T_i} + \left(\zeta_{31} + \zeta_{32}\nu_{s,i} + \frac{\zeta_{33}}{\nu_{s,i}} + \zeta_{34}\ln(\nu_{s,i})\right)\ln(T_i) \quad (1)$$

where T_i represents the crystallizer temperature in stage i, $\nu_{s,i}$ is the solvent volume fraction in the crystallizer at stage i, and values for each solubility parameter, ζ_{kl}, are presented in Table 1. The solvent volume fractions are defined on an API-free basis as: (volume of THF + volume of EtOH)/(volume of THF + volume of EtOH + volume of water).

In this work, supersaturation in the ith stage, σ_i, is expressed as

$$\sigma_i = \ln\left(\frac{c_i}{c_i^*}\right) \quad (2)$$

where the saturation concentration in each stage is calculated using the solubility expression provided in eq 1. By employing this supersaturation expression, the same kinetic prefactors and growth factors may be used from previous research on the API of interest.[24]

Table 1. Solubility Parameter (ζ_{kl}) Values[a]

$k \downarrow / l \rightarrow$	1	2	3	4
1	−8070.4	12 537.09	−4972.05	−16 622.6
2	339 770.2	−531 620	212 470.6	708 640.1
3	1219.833	−1892.13	749.4551	2507.269

[a]The calculated solubilities have units of g API/kg solution.

DOI: 10.1021/acs.oprd.9b00244
Org. Process Res. Dev. 2019, 23, 1960−1969

API kinetics are assumed to follow a power law form for growth

$$G_i = k_{g,i}\sigma_i^{g_i} \tag{3}$$

where G_i, $k_{g,i}$, and g_i are the growth rate, lumped growth prefactor, and growth power in stage i, respectively.

Similarly, for nucleation

$$B_i = k_{b,i}\sigma_i^{b_i}\frac{\mu_3^{(i)}}{3G_i\tau_i} \tag{4}$$

where B_i is the nucleation rate in the ith stage, $k_{b,i}$ is the nucleation prefactor in the ith crystallizer, is the nucleation power in the ith stage, τ_i is the residence time in stage i, and $\mu_3^{(i)}$ is the third moment of the crystal population in stage i. This expression for API nucleation assumes that secondary nucleation is the predominant nucleation mechanism in each MSMPR crystallizer. Previous research also indicates that API crystal growth kinetics exhibit substantial solvent dependence and temperature dependence.[24] This functionality is estimated to have the following form

$$k_{g,i} = k_{g0,i}\exp\left(\frac{-k_{g1,i}}{T_i}\right) \tag{5}$$

$$k_{g1,i} = 3104\exp(-0.86v_{s,i}) \tag{6}$$

$$k_{g0,i} = 0.0207\exp(-8.395v_{s,i}) \tag{7}$$

$$g_i = 1 \tag{8}$$

For these expressions, $k_{g0,i}$ and $k_{g1,i}$ are the growth prefactor and growth activation prefactor in stage i, respectively.

Similarly, previous research indicates that API crystal nucleation kinetics exhibit strong solvent dependence but minor temperature dependence.[24] For this reason, temperature-dependent nucleation kinetics are neglected, and the functional form of crystal nucleation is estimated as follows

$$k_{b,i} = \begin{cases} -61316250(v_{s,i} - 0.44) + 3892050 & \text{for } v_{s,i} \le 0.48 \\ -1266277\,(v_{s,i} - 0.48) + 1439400 & \text{for } v_{s,i} > 0.48 \end{cases} \tag{9}$$

$$b_i = 2 \tag{10}$$

By incorporating the solvent and temperature dependence of the kinetic prefactors, crystallizer cascade performance can be more accurately predicted.

Multistage MSMPR Model. Continuous steady-state N-stage MSMPR cascade systems were simulated in MATLAB using population balance equations, where N = 1, 2, or 3 stages. In using this population balance modeling scheme, the following assumptions are made:

1. The feed solution contains no crystals.
2. The mixing of solvent and antisolvent does not affect the total solution volume, and the crystalline phase has a negligible contribution to the total suspension volume.
3. All crystals nucleate from a size of 0 μm.
4. There is no growth dispersion or size-dependent growth, and the crystal shape factor is independent of kinetics and solvent composition.
5. Crystals experience negligible agglomeration and breakage in the crystallizer.
6. Each crystallizer is well-mixed, so the outlet of the crystallizer has the same composition as the crystallizer contents.
7. All crystallization occurs within the cascade crystallizers.
8. All crystallizers operate at steady state.

There are four main parts of the steady-state crystallization model: an API material balance, a population balance, and two kinetic expressions, one for crystal nucleation and one for crystal growth. In this work, we chose to optimize the crystallization cascades based on the steady-state moments of the crystal population. Based on the previous assumptions and because clear feed enters the first crystallizer, the zeroth moment of the first crystallizer is

$$0 = -\frac{1}{\tau_1}\mu_0^{(1)} + B_1 \tag{11}$$

and

$$0 = \frac{1}{\alpha_{mf,i}\tau_{i-1}}\mu_0^{(i-1)} - \frac{1}{\tau_i}\mu_0^{(i)} + B_i \tag{12}$$

in each additional crystallizer, where

$$\mu_j^{(i)} = \int_0^\infty L^j n_i(L)\mathrm{d}L \tag{13}$$

represents the jth moment at stage i, L is the characteristic crystal length, and n_i is the population density at stage i.[6] Similarly, the first- and higher-order moments are

$$0 = -\frac{1}{\tau_1}\mu_j^{(1)} + jG_1\mu_{j-1}^{(1)} \tag{14}$$

in the first stage and

$$0 = \frac{1}{\alpha_{mf,i}\tau_{i-1}}\mu_j^{(i-1)} - \frac{1}{\tau_i}\mu_j^{(i)} + jG_i\mu_{j-1}^{(i)} \tag{15}$$

in each successive stage. In these population balance equations

$$\alpha_{mf,i} = \frac{\rho_{soln,i}}{\alpha_i\rho_{soln,i-1}} \tag{16}$$

is the mass-based dilution factor and

$$\alpha_i = \frac{v_{s,i}}{v_{s,i-1}} \tag{17}$$

is the volume-based dilution factor, where

$$\rho_{soln,i} = \alpha_i\rho_{soln,i-1} + (1 - \alpha_i)\rho_{AS} \tag{18}$$

describes the density of the solvent mixture in stage i. In these expressions, ρ_{AS} represents the density of the antisolvent.

The simplified material balance governing the API in the crystallizer is described by[18]

$$0 = \frac{c_{i-1}}{\alpha_{mf,i}\tau_{i-1}} - \frac{c_i}{\tau_i} - 3k_v\rho_c G_i\mu_2^{(i)} \tag{19}$$

where c_i is the API concentration in the ith stage. For this system, the shape factor, k_v, and crystal density, ρ_c, are assumed to be constants with values of 0.21 and 1.228 kg/m^3, respectively. Finally, the kinetic expressions for API nucleation and growth are the same expressions provided in eqs 3 and 4, where the kinetic prefactors and powers are those described in eqs 5−10. A consolidated statement of this MSMPR model is provided in the Supporting Information.

DOI: 10.1021/acs.oprd.9b00244
Org. Process Res. Dev. 2019, 23, 1960−1969

Table 2. Conditions for One-, Two-, and Three-Stage Steady-State MSMPR Cascade Simulations

stage	T_{min} (°C)	T_{step} (°C)	T_{max} (°C)	$\nu_{s,min}$	$\nu_{s,step}$	$\nu_{s,max}$	τ_{min} (min)	τ_{step} (min)	τ_{max} (min)
Single-Stage (273 060 Simulations)									
1	10	0.5	30	0.44	0.0025	0.90	5	5	180
Two-Stage (874 800 Simulations)									
1	10	2.5	30	0.44	0.02	0.90	20	20	160
2	10	2.5	30	0.44	0.01	0.90	20	20	160
Three-Stage (490 500 Simulations)									
1	10	10	30	0.44	0.046	0.90	20	40	140
2	10	10	30	0.44	0.046	0.90	20	40	140
3	10	5	30	0.44	0.02	0.90	20	40	140

Process Constraints. For the studied system, there are a number of specifications, which are placed on the final crystallized product by the manufacturer. The following specifications must be met during the crystallization process:

1. The yield must equal or exceed 90% exiting the final crystallizer: $Y \geq 0.90$.
2. The d_{50} of the crystal size distribution (CSD) must equal or exceed 40 μm exiting the final crystallizer: $d_{50} \leq 40$ μm.
3. The d_{90} of the CSD must not exceed 240 μm exiting the final crystallizer: $d_{90} \leq 240$ μm.

These specifications provide the minimum set of constraints on the final product quality, which are specified by the manufacturer. Though more rigorous constraints on CSD or mean crystal size could be imposed, those constraints are outside of the scope of the optimization presented in this report. The primary goal of the current optimization is to maximize API yield.

Aside from these specifications on the final crystallized product, the process operating conditions have also been constrained:

1. API feed enters the first crystallizer at a temperature of 55 °C and a concentration of 70 g/kg solution (on an antisolvent-free basis): $c_0 = 70$ g/kg.
2. The solvent fraction of the feed stream is 100% solvent (on an API-free basis): $\alpha_0 = 1$.
3. The solvent fraction must not exceed 90 vol % and must not be reduced below 44 vol % in any crystallizer: $0.44 \leq \upsilon_{s,i} \leq 0.90$.
4. The solvent fraction must remain the same or decrease in each stage: $\nu_{s,i} < \nu_{s,i-1}$.
5. Each crystallizer temperature cannot exceed 30 °C and may not be colder than 10 °C: 10 °C $\leq T_i \leq$ 30 °C.
6. The total residence time of the crystallization cascade cannot exceed 3 h: $\sum_{i=1}^{N} \tau_i = \tau_{tot} \leq 180$ min.

A consolidated statement of the MSMPR model along with these process constraints is provided in the Supporting Information.

MSMPR Cascade Simulations. To estimate the optimal API processing conditions for the one, two, or three-stage MSMPR cascades, thousands of sets of reactor operating conditions were considered to approximate the solution to the following optimization problem

$$\max_{T_i,\nu_i,\tau_i} Y \tag{20}$$

subject to the previous process constrains, where Y is the yield, expressed as

$$Y = \frac{C_0\alpha_{mf,end} - C_{end}}{C_0\alpha_{mf,end}} \tag{21}$$

Temperature, solvent composition, and residence time are selected for each crystallization stage to comprise the set of operating conditions. Based on the number of stages in the cascade, the step size for each of these process variables was varied to restrict the number of crystallizers that were simulated. The variation in operating conditions used for each cascade simulation is provided in Table 2. For each set of operating conditions, each crystallizer was modeled using the MSMPR steady-state cascade model subject to the process constraints, which are outlined in the Process Constraints section. Based on the yield and mean volume particle size ($L_{4,3}$) for each simulated crystallization cascade, the attainable region associated with the parameter space was mapped. For this work, the volume-averaged mean size is calculated according to the following equation

$$L_{4,3} = \frac{\int_0^\infty nL^4\,dL}{\int_0^\infty nL^3\,dL} = \frac{\mu_4}{\mu_3} \tag{22}$$

where $L_{4,3}$ is the volume-averaged mean size, n is the crystal number density, and L is the size of the characteristic crystal dimension.

To compare crystallizer performance to the performance of crystallizer cascades with additional constraints that are commonly assumed for cooling and/or antisolvent crystallizations, the crystallizer simulations were replicated with one additional type of constraint or heuristic imposed. First, the optimization was again completed using solvent-independent kinetics (SIK) for the cases of the one-, two-, and three-stage cascades. For the case of solvent-independent kinetics, k_b and k_g were calculated as constants, assuming that kinetics were measured at a solvent composition of $\nu_s = 0.48$. At solvent fractions below $\nu_s = 0.48$, the solubility curve is fairly flat. Therefore, $\nu_s = 0.48$ is the most likely choice of solvent composition if the operating solvent composition was chosen based on the solubility data alone. Next, the MSMPR cascade optimization was repeated using solvent-dependent kinetics for the two- and three-stage cascades, where equal antisolvent addition was required in each stage. Finally, the simulation was repeated for the two-stage MSMPR cascade where the temperature was required to stay constant or decrease in the second stage. The mathematical statements associated with each of these additionally imposed process constraints are provided in the Supporting Information.

DOI: 10.1021/acs.oprd.9b00244
Org. Process Res. Dev. 2019, 23, 1960−1969

Table 3. Optimization Results for the Steady-State MSMPR Cascades

number of cascade stages/simulation type	T_1 (°C)	T_2 (°C)	T_3 (°C)	$\nu_{s,1}$	$\nu_{s,2}$	$\nu_{s,3}$	τ_1 (min)	τ_2 (min)	τ_3 (min)	Y (wt %)	$L_{4,3}$ (μm)
Single-Stage											
solvent-dependent kinetics	10			0.44			160			97.08	142.9
solvent-independent kinetics	10			0.44			70			90.52	143.0
Two-Stage											
solvent-dependent kinetics	10	10		0.44	0.44		100	80		99.47	127.0
solvent-independent kinetics	10	10		0.44	0.44		60	120		99.43	137.6
equal volumes of antisolvent addition	10	10		0.61	0.44		80	100		98.66	129.3
Three-Stage											
solvent-dependent kinetics	10	10	10	0.44	0.44	0.44	60	60	60	99.49	111.8
solvent-independent kinetics	10	10	10	0.44	0.44	0.44	60	60	60	99.49	137.6
equal volumes of antisolvent addition	10	10	10	0.70	0.54	0.44	20	60	100	98.99	129.8

Table 4. Steady-State MSMPR Cascade Simulation Results with Refined Residence Time

number of cascade stages	T_1 (°C)	T_2 (°C)	T_3 (°C)	$\nu_{s,1}$	$\nu_{s,2}$	$\nu_{s,3}$	τ_1 (min)	τ_2 (min)	τ_3 (min)	Y (wt %)	$L_{4,3}$ (μm)
1	10			0.44			163			97.11	143.5
2	10	10		0.44	0.44		93	87		99.47	124.7
3	10	10	10	0.44	0.44	0.44	63	60	57	99.49	113.2

RESULTS AND DISCUSSION

Cascade Optimization Results. Results of the simulations for optimal operating conditions in the one-, two-, and three-stage crystallization cascades are provided in Table 3. When solvent-dependent kinetics are considered, the optimal operation occurs at the lowest temperature and the lowest solvent fraction for each crystallizer in the cascade, regardless of the number of stages. This means that the antisolvent addition occurs only on the first stage. The selection of the lowest solvent fraction results from two cooperating phenomena: (1) from a thermodynamic perspective, an increase in supersaturation results from minimizing solubility at low solvent fractions and (2) from a kinetic perspective, there is an exponential increase in prefactors k_b and k_g at low solvent fractions.

Both of these phenomena work to increase the growth and nucleation rates, leading to increased yield. The selection of the lowest temperature for each stage occurs because the resulting increase in the growth and nucleation rates from lowering the API solubility (and, thereby, increasing supersaturation) is not offset by the retardation in kinetics from reduced temperatures. Residence time appears to be split approximately equally among the crystallizers in the multistage cascades but is limited for the single-stage case.

Repeating the cascade simulation in the vicinity of the low solvent fraction and low temperature indicates that residence time is optimally split almost equally between each of the crystallizers in the cascades, with earlier stages requiring slightly more residence time for maximum yield. These results are provided in Table 4, where the optimal residence time in each stage was determined within ±1 min.

As the number of stages in the MSMPR cascade increases, the yield increases. However, the mean particle size associated with the highest yield decreases with an increasing number of cascade stages. Though the results indicate that the highest yield can be obtained in a three-stage crystallizer, there is only a little increase in yield when transitioning from a two-stage MSMPR cascade to a three-stage MSMPR cascade at optimal operating conditions. Furthermore, it is possible to meet all particle size and yield specifications in a single crystallizer. Therefore, the use of multiple MSMPR crystallizers in a cascade is not necessarily required for this process. Figure 2 confirms these findings. Figure 2a shows that as the number of stages increases, the volumetric particle size distribution shifts slightly to the left toward lower mean particle sizes. However, the attainable region greatly expands once multiple MSMPR crystallizers are used in a cascade, as shown in Figure 2b. Having the ability to operate at different temperatures and solvent compositions in each stage of the MSMPR cascade expands the steady-state process design space. As nucleation and growth rates vary as functions of the solvent composition, tuning the solvent composition in each stage of an MSMPR cascade allows a variety of final product attributes to be achieved using a small number of MSMPR crystallizers in the cascade. For example, the attainable region expands greatly

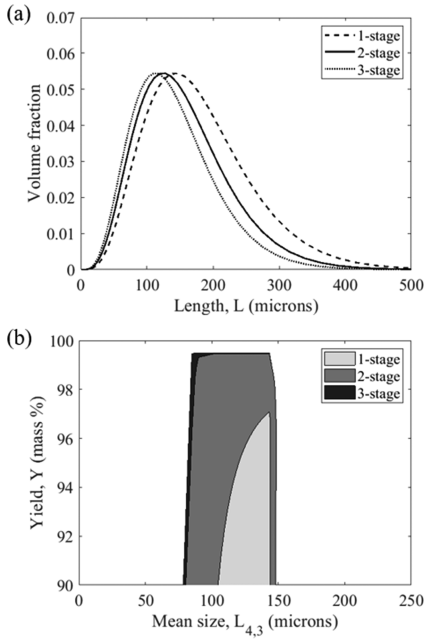

Figure 2. Volume-based CSD (a) at optimal MSMPR operating conditions and attainable region (b) for the one-, two-, and three-stage MSMPR cascade.

DOI: 10.1021/acs.oprd.9b00244
Org. Process Res. Dev. 2019, 23, 1960−1969

when shifting from using one MSMPR to using two MSMPRs in the cascade. In particular, lower mean particle sizes are achievable in the two-stage MSMPR cascade, when compared with a single MSMPR crystallizer. Maximum yield is increased for the multistage MSMPR cascade, as well. The area of the attainable region expands again when transitioning from the two-stage to the three-stage crystallization process, though there are diminishing returns for adding a third crystallizer to the cascade. If at least two stages are used in the MSMPR cascade, then a high yield and mean size can be selected independently by choosing the proper set of operating conditions (temperature, solvent fraction, and residence time). For these reasons, it may be preferable to use two stages instead of a single-stage MSMPR cascade. It is unlikely that more than two MSMPRs would be required for this process.

Influence of Solvent-Dependent Kinetics on Single-Stage MSMPR Simulations. The first evaluation was on the influence of including solvent-dependent kinetics on the calculated attainable region and the volumetric size distribution of the particles exiting the crystallizer in a single-stage MSMPR. Figure 3a indicates that the attainable region that

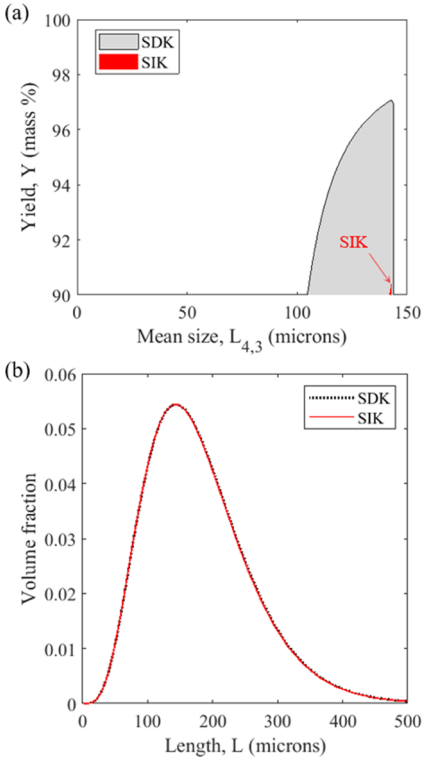

Figure 3. Attainable region (a) and volume-based CSD at optimal MSMPR operating conditions (b) for cases of solvent-dependent kinetics (SDK) and solvent-independent kinetics (SIK) in a single MSMPR.

incorporates solvent-dependent kinetics is much larger than would be predicted if it was erroneously assumed that the kinetics were solvent-independent. The attainable region area is expanded because the growth and nucleation rates are much larger at lower solvent fractions with the solvent-dependent kinetics. If the volumetric particle size distributions are considered, they do not change with incorporating solvent-dependent versus solvent-independent kinetics (Figure 3b). This is expected, as the broadness of a CSD in an ideal, single-stage MSMPR is determined by the residence time distribution, which is the same in both cases. However, note that this distribution is normalized, and the number of particles in each size range is greatly increased when solvent-dependent kinetics are incorporated. In fact, the yield is predicted to be almost 6.6% higher if solvent-dependent kinetics are incorporated in the MSMPR model (Table 3).

Including solvent-dependent kinetics also reduces the expected mean particle size slightly in the single-stage case. This trend is also seen in the two- and three-stage cases and will be discussed further.

Influence of Solvent-Dependent Kinetics on Two-Stage MSMPR Simulations. Figure 4a shows the effect of

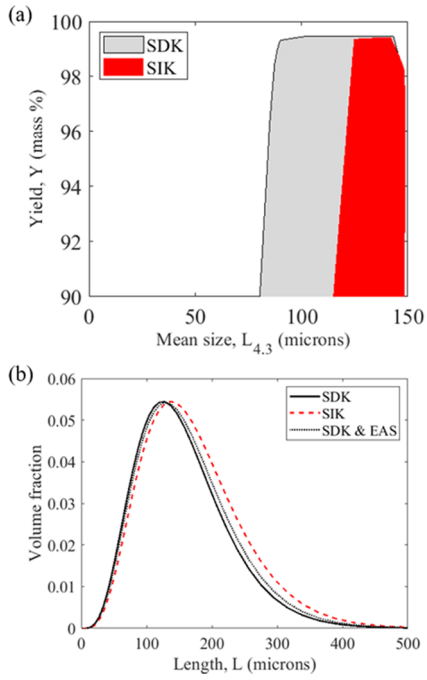

Figure 4. Attainable region (a) and volume-based CSD at optimal MSMPR operating conditions (b) for cases of solvent-dependent kinetics (SDK) and solvent-independent kinetics (SIK) in a two-stage MSMPR cascade. The volume-based CSD at optimal MSMPR operating conditions is also displayed for the case of equal antisolvent addition (EAS).

neglecting solvent-dependent kinetics when simulating the attainable region for the two-stage MSMPR cascade. If the dependence on the solvent is neglected, then the attainable region appears to be less than half the size than would otherwise be simulated. Though similar maximum yields are predicted, lower mean sizes are not seen as being achievable if the solvent-dependent kinetics are excluded. Similarly, the CSD associated with the maximum yield shifts left when the solvent-dependent kinetics are included (Figure 4b). Lower mean sizes are obtained because the nucleation rates at the optimal solvent fraction are higher in the case of solvent-dependent versus solvent-independent kinetics, leading to greater mass deposition for crystal nucleation.

Influence of Solvent-Dependent Kinetics on Three-Stage MSMPR Simulations. Though maximum yield achievable in the three-stage cascade is only marginally better than in the two-stage cascade, it is worth considering what happens if solvent-independent rather than solvent-dependent kinetics are used to model the three-stage MSMPR cascade.

DOI: 10.1021/acs.oprd.9b00244
Org. Process Res. Dev. 2019, 23, 1960−1969

Similar to the two-stage cascade, Figure 5a indicates that neglecting the solvent-dependent kinetics drastically reduces the area of the attainable region. Figure 5b shows the differences in the volumetric CSD for the cases where solvent-dependent kinetics are incorporated or neglected for the three-stage MSMPR cascade and confirms the findings that are shown in Table 3. Again, the mean size is overpredicted and the yield is underpredicted at the optimal set of operating conditions.

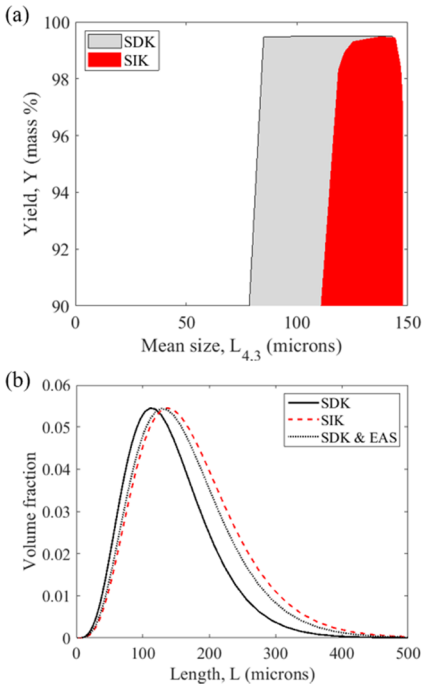

Figure 5. Attainable region (a) and volume-based CSD at optimal MSMPR operating conditions (b) for cases of solvent-dependent kinetics (SDK) and solvent-independent kinetics (SIK) in a three-stage MSMPR cascade. The volume-based CSD at optimal MSMPR operating conditions is also displayed for the case of equal antisolvent addition (EAS).

Regardless of the number of stages simulated in the MSMPR cascade, incorporating solvent-dependent kinetics is of extreme importance. Neglecting the dependence of the kinetics on the solvent composition leads to substantial differences in calculating API yield, mean size, CSD, and the attainable region in each cascade.

Shortcomings of Common Antisolvent Crystallization Heuristics. Beyond using solvent-independent instead of solvent-dependent kinetics, there are a number of common heuristics that are used in simulating crystallization cascades with antisolvent crystallization or CCAC. It was decided to compare the attainable regions, which one would obtain using these common heuristics, to the attainable regions obtained if no additional constraints beyond the yield and CSD constraints were imposed on the crystallizer cascade performance.

For example, a common heuristic for designing antisolvent crystallization processes is to require equal antisolvent addition in each stage. If the constraint of equal antisolvent addition is imposed, the attainable region shrinks drastically, and the maximum yield achievable in the process is reduced. Furthermore, the smaller mean sizes are not achievable. This is shown in Figure 6. Although direct restrictions or constraints on the mean size were not imposed, it may preferable based on downstream processing requirements to aim for a smaller mean size, especially for high-potency APIs. Therefore, requiring equal antisolvent addition is unnecessary and restricts the attainable final product mean size exiting the final crystallizer.

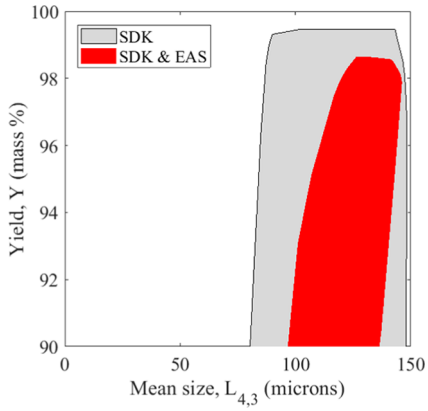

Figure 6. Comparison of attainable region area for the mean size and yield if equal antisolvent volume addition (EAS) in each stage is imposed as a process constraint for the two-stage MSMPR cascade.

Another common approach for determining the attainable region for antisolvent crystallizers and selecting operating conditions includes implementing a constraint that requires the temperature in each stage to be less than or equal to the temperature in the preceding stage. This is the most common constraint used in cooling and CCAC crystallizations. In Figure 7, it is shown how this restriction affects the attainable region. The area of the attainable region is approximately unchanged because the boundaries of the attainable region are not formed at operating conditions where the temperatures in successive stages are higher than the preceding stages. For example, at the top yields achievable, the temperatures are equal in each stage. Though implementing this constraint of decreasing the temperature in each additional stage would have reduced the computational time to solve the optimization problem, this constraint is unnecessary and may lead to false conclusions based on the other constraints selected for operating conditions.

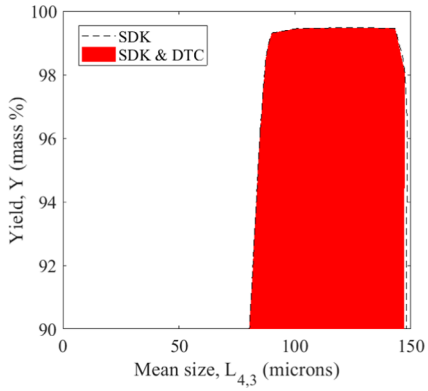

Figure 7. Comparison of the attainable region area for the mean size and yield if a decreasing temperature constraint is imposed in the two-stage MSMPR cascade.

DOI: 10.1021/acs.oprd.9b00244
Org. Process Res. Dev. 2019, 23, 1960−1969

At high total residence times in the two-stage MSMPR cascade, there is a plateau in the maximum yield achievable (Figure 8). If the total residence time in the system was restricted to be substantially smaller than 180 min, the attainable region would change such that it may be beneficial to increase the temperature in successive stages. For this particular system, an example of such a case occurs when an objective is to maximize the production rate instead of simply maximizing the yield in the final crystallization stage.

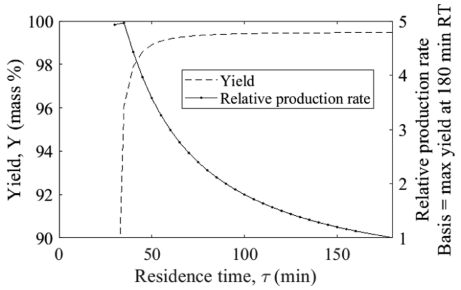

Figure 8. Yield and relative production rate as a function of the total residence time allowed in the two-stage MSMPR cascade. Maximum production occurs at a total residence time of approximately 35 min.

As it can be seen from Figure 8, reducing the total residence time to approximately 35 min can lead to significant gains in the production rate (defined in kg/min of the generated solid API, relative to the crystallizer size) against the conditions of maximum yield at 180 min residence time.

At low residence times, the optimal residence time is split unevenly between the two stages and favors increasing the temperature from 25 °C in the first stage to 30 °C in the second stage to compensate for the limited residence time (Table 5). This is due to the tradeoff that occurs in the growth and nucleation rates due to changes in temperature. Temperature affects growth and nucleation rates in two ways. As the temperature is increased, growth and nucleation rates increase due to the increase in the kinetic prefactors, k_b and k_g. However, temperature increases also increase the solubility in the system, leading to a kinetic inhibition from lower operating supersaturations as well as lower solids concentration at the same residence time. In the limit of low residence times in the multistage crystallizer cascade, the reduction in supersaturation from the increased temperature is more than offset by the increase in growth and nucleation rates from increasing the kinetic prefactors. Therefore, if a process objective is to maximize the production rate instead of yield, it is beneficial to remove the limitation that the temperature must remain the same or decrease in each successive stage.

Ultimately, neither of the two commonly used crystallizer cascade design heuristics for antisolvent crystallization should be used for systems where the growth and nucleation kinetics are solvent-dependent.

CONCLUSIONS

In this work, a series of steady-state MSMPR cascades was simulated to evaluate the effect of incorporating solvent-dependent kinetics in antisolvent crystallization process design. Antisolvent crystallization cascade design should account for effects of the solvent composition on crystallization kinetics. Failure to include solvent-dependent kinetics could result in the simulation of incorrect attainable regions, API yields, crystal morphologies, and CSDs. In multistage crystallization cascades, the selection of the solvent composition may have a stronger influence on the attainable product attributes than other process operating conditions such as temperature or residence time.

Beyond demonstrating the need to include solvent-dependent kinetics in antisolvent crystallizer designs, it was also demonstrated that some of the commonly employed crystallization process design heuristics should not be used for processes that have strongly solvent-dependent kinetics. For processes where it is beneficial to constrain the mean particle size, requiring equal antisolvent addition can prevent the lowest mean particle sizes from being obtained at high yields. It was also demonstrated that constraining the temperature in the crystallizer to remain the same or decrease in each successive MSMPR in the cascade is another unnecessary process constraint. For processes where a maximum production rate at high yield is preferred to maximum yield, it may be beneficial to operate the crystallizer cascade by increasing the temperature in later stages, especially in the limit of short residence times.

ASSOCIATED CONTENT

Supporting Information

The Supporting Information is available free of charge on the ACS Publications website at DOI: 10.1021/acs.oprd.9b00244.

Consolidated statement for the mathematical models; additional process constraints for the evaluation of optimization heuristics (PDF)

(PDF)

Table 5. Optimal Operating Conditions for a Two-Stage MSMPR Cascade with Selected τ_1, τ_2

T_1 (°C)	T_2 (°C)	$\nu_{s,1}$	$\nu_{s,2}$	τ_1 (min)	τ_2 (min)	τ_{tot} (min)	Y (wt %)	relative production rate	$L_{4,3}$ (μm)
10	10	0.44	0.44	80	80	160	99.47	1.12	120.1
10	10	0.44	0.44	65	55	120	99.44	1.50	114.0
10	10	0.44	0.44	50	30	80	99.36	2.25	106.8
10	10	0.44	0.44	40	20	60	99.18	2.99	101.0
10	10	0.44	0.44	35	20	55	99.08	3.26	97.7
10	10	0.44	0.44	35	15	50	98.90	3.58	97.7
10	10	0.44	0.44	30	15	45	98.59	3.96	93.9
15	17.5	0.44	0.44	25	15	40	97.89	4.43	95.7
25	30	0.44	0.44	20	15	35	96.08	4.97	102.5
30	30	0.44	0.44	15	15	30	81.76	4.93	101.3

DOI: 10.1021/acs.oprd.9b00244
Org. Process Res. Dev. 2019, 23, 1960−1969

AUTHOR INFORMATION

Corresponding Author

*E-mail: myerson@mit.edu.

ORCID

Gerard Capellades: 0000-0002-4056-3823
Richard D. Braatz: 0000-0003-4304-3484
Allan S. Myerson: 0000-0002-7468-8093

Author Contributions

The manuscript was written through contributions of all of the authors. All of the authors have given approval to the final version of the manuscript.

Notes

The authors declare no competing financial interest.

ACKNOWLEDGMENTS

We thank the Novartis-MIT Center for Continuous Manufacturing for funding and technical guidance. We also acknowledge the National Science Foundation, Grant no. 1122374, for funding. Any opinion, findings, and conclusions or recommendations expressed in this material are those of the authors and do not necessarily reflect the views of the National Science Foundation.

NOMENCLATURE

B_i, nucleation rate at the ith stage, kg/min
b_i, nucleation power in ith crystallizer
c_i, API concentration in the liquid phase of the ith stage crystallizer, kg/kg solution
c_i^*, saturation concentration in ith crystallizer, kg/kg solution
c_0, inlet API concentration, kg/kg solution
G_i, growth rate at the ith stage, μm/min
g_i, growth power in ith crystallizer
i, stage number
j, moment number
$k_{b,i}$, nucleation prefactor in ith crystallizer, μm^2/min
$k_{g,i}$, lumped growth prefactor in ith crystallizer, μm/min
$k_{g0,i}$, growth prefactor in ith crystallizer, μm/min
$k_{b1,i}$, growth activation prefactor in ith crystallizer, K
k_v, volume shape factor
L, characteristic crystal length, μm
$L_{4,3}$, volume-based mean crystal size, μm
n_i, number density at stage i, μm/kg
T_i, temperature in ith crystallizer, K
$v_{s,i}$, solvent volume fraction (mL solvent/mL solvent + antisolvent) in stage i
Y, yield, %
α_i, volume-based dilution factor at the ith stage
$\alpha_{mf,i}$, mass-based dilution factor at the ith stage
$\mu_j^{(i)}$, jth moment in the ith stage, μm^j/kg
ζ_{kl}, solubility parameter
ρ_{AS}, antisolvent density, kg/m^3
ρ_c, crystal density, kg/μm^3
ρ_{soln}, solution density, kg/m^3
σ_i, supersaturation in ith crystallizer
τ_i, residence time at the ith stage, min
τ_{tot}, total residence time for crystallization process, min

REFERENCES

(1) Howard, K. S.; Nagy, Z. K.; Saha, B.; Robertson, A. L.; Steele, G.; Martin, D. A Process Analytical Technology Based Investigation of the Polymorphic Transformations during the Antisolvent Crystallization of Sodium Benzoate from IPA/Water Mixture. *Cryst. Growth Des.* **2009**, *9*, 3964−3975.

(2) Takiyama, H.; Minamisono, T.; Osada, Y.; Matsuoka, M. Operation Design for Controlling Polymorphism in the Anti-Solvent Crystallization by Using Ternary Phase Diagram. *Chem. Eng. Res. Des.* **2010**, *88*, 1242−1247.

(3) Albright, L. F. *Albright's Chemical Engineering Handbook*; CRC Press: Boca Raton, 2009.

(4) Giulietti, M.; Seckler, M.; Derenzo, S.; Ré, M.; Cekinski, E. Industrial Crystallization and Precipitation from Solutions: State of the Technique. *Braz. J. Chem. Eng.* **2001**, *18*, 423−440.

(5) Yang, Y.; Nagy, Z. K. Model-Based Systematic Design and Analysis Approach for Unseeded Combined Cooling and Antisolvent Crystallization (CCAC) Systems. *Cryst. Growth Des.* **2014**, *14*, 687−698.

(6) Randolph, A. D.; Larson, M. A. *Theory of Particulate Processes: Analysis and Techniques of Continuous Crystallization*; Academic Press: London, 1971.

(7) Quon, J. L.; Zhang, H.; Alvarez, A.; Evans, J.; Myerson, A. S.; Trout, B. L. Continuous Crystallization of Aliskiren Hemifumarate. *Cryst. Growth Des.* **2012**, *12*, 3036−3044.

(8) Plumb, K. Continuous Processing in the Pharmaceutical Industry. *Chem. Eng. Res. Des.* **2005**, *83*, 730−738.

(9) Alvarez, A. J.; Myerson, A. S. Continuous Plug Flow Crystallization of Pharmaceutical Compounds. *Cryst. Growth Des.* **2010**, *10*, 2219−2228.

(10) Cervera-Padrell, A. E.; Skovby, T.; Kiil, S.; Gani, R.; Gernaey, K. V. Active Pharmaceutical Ingredient (API) Production Involving Continuous Processes - A Process System Engineering (PSE)-Assisted Design Framework. *Eur. J. Pharm. Biopharm.* **2012**, *82*, 437−456.

(11) Vervaet, C.; Remon, J. P. Continuous Granulation in the Pharmaceutical Industry. *Chem. Eng. Sci.* **2005**, *60*, 3949−3957.

(12) Lindenberg, C. *Optimizing the Precipitation of Organic Compounds*; Swiss Federal Institute of Technology: Zürich, 2009.

(13) Lai, T.-T. C.; Cornevin, J.; Ferguson, S.; Li, N.; Trout, B. L.; Myerson, A. S. Control of Polymorphism in Continuous Crystallization via Mixed Suspension Mixed Product Removal Systems Cascade Design. *Cryst. Growth Des.* **2015**, *15*, 3374−3382.

(14) Ferguson, S.; Ortner, F.; Quon, J.; Peeva, L.; Livingston, A.; Trout, B. L.; Myerson, A. S. Use of Continuous MSMPR Crystallization with Integrated Nanofiltration Membrane Recycle for Enhanced Yield and Purity in API Crystallization. *Cryst. Growth Des.* **2014**, *14*, 617−627.

(15) Ferguson, S.; Morris, G.; Hao, H.; Barrett, M.; Glennon, B. Characterization of the Anti-Solvent Batch, Plug Flow and MSMPR Crystallization of Benzoic Acid. *Chem. Eng. Sci.* **2013**, *104*, 44−54.

(16) Park, K.; Kim, D. Y.; Yang, D. R. Operating Strategy for Continuous Multistage Mixed Suspension and Mixed Product Removal (MSMPR) Crystallization Processes Depending on Crystallization Kinetic Parameters. *Ind. Eng. Chem. Res.* **2016**, *55*, 7142−7153.

(17) Kee, N. C. S.; Arendt, P. D.; Goh, L. M.; Tan, R. B. H.; Braatz, R. D. Nucleation and Growth Kinetics Estimation for L-Phenylalanine Hydrate and Anhydrate Crystallization. *CrystEngComm* **2011**, *13*, 1197−1209.

(18) Yang, Y.; Nagy, Z. K. Combined Cooling and Antisolvent Crystallization in Continuous Mixed Suspension, Mixed Product Removal Cascade Crystallizers: Steady-State and Startup Optimization. *Ind. Eng. Chem. Res.* **2015**, *54*, 5673−5682.

(19) Vetter, T.; Burcham, C. L.; Doherty, M. F. Regions of Attainable Particle Sizes in Continuous and Batch Crystallization Processes. *Chem. Eng. Sci.* **2014**, *106*, 167−180.

(20) Wong, S. Y.; Tatusko, A. P.; Trout, B. L.; Myerson, A. S. Development of Continuous Crystallization Processes Using a Single-Stage Mixed-Suspension, Mixed-Product Removal Crystallizer with Recycle. *Cryst. Growth Des.* **2012**, *12*, 5701−5707.

(21) Da Rosa, C. A.; Braatz, R. D. OpenCrys: Open-Source Software for the Multiscale Modeling of Combined Antisolvent and Cooling

DOI: 10.1021/acs.oprd.9b00244
Org. Process Res. Dev. 2019, 23, 1960−1969

Crystallization in Turbulent Flow. *Ind. Eng. Chem. Res.* **2018**, *57*, 11702−11711.
(22) Zhang, H.; Quon, J.; Alvarez, A. J.; Evans, J.; Myerson, A. S.; Trout, B. Development of Continuous Anti-Solvent/Cooling Crystallization Process Using Cascaded Mixed Suspension, Mixed Product Removal Crystallizers. *Org. Process Res. Dev.* **2012**, *16*, 915−924.
(23) Garg, M.; Roy, M.; Chokshi, P.; Rathore, A. S. Process Development in the QbD Paradigm: Mechanistic Modeling of Antisolvent Crystallization for Production of Pharmaceuticals. *Cryst. Growth Des.* **2018**, *18*, 3352−3359.
(24) Schall, J. M.; Mandur, J. S.; Braatz, R. D.; Myerson, A. S. Nucleation and Growth Kinetics for Combined Cooling and Antisolvent Crystallization in a Mixed-Suspension, Mixed-Product Removal System: Estimating Solvent Dependency. *Cryst. Growth Des.* **2018**, *18*, 1560−1570.
(25) Power, G.; Hou, G.; Kamaraju, V. K.; Morris, G.; Zhao, Y.; Glennon, B. Design and Optimization of a Multistage Continuous Cooling Mixed Suspension, Mixed Product Removal Crystallizer. *Chem. Eng. Sci.* **2015**, *133*, 125−139.
(26) Nagy, Z. K.; Fujiwara, M.; Braatz, R. D. Modelling and Control of Combined Cooling and Antisolvent Crystallization Processes. *J. Process Control* **2008**, *18*, 856−864.

DOI: 10.1021/acs.oprd.9b00244
Org. Process Res. Dev. 2019, 23, 1960−1969